Optimized Routine of Machining Distortion Characterization Based on Gaussian Surface Curvature

Destiny R. Garcia
Mechanical and Aerospace Engineering Department, University of California Davis, CA, USA

Barbara S. Linke[1]
Mechanical and Aerospace Engineering Department, University of California Davis, CA, USA

Rida T. Farouki
Mechanical and Aerospace Engineering Department, University of California Davis, CA, USA

Abstract

Machining distortion presents a significant problem in products with high residual stresses from materials processing and re-equilibration after machining removes a large part of the material volume and is common in the aerospace industries. While many papers research on mechanisms of machining distortion, few papers report on the measurement, processing and characterization of distortion data. Oftentimes only line plot data is used to give a maximum distortion value. This paper proposes a method of measurement tool selection, measurement parameter selection, data processing through filtering and leveling, and use of Bézier Surfaces and Gaussian Curvature for distortion characterization. The method is demonstrated with three sample pieces of different pocket geometry from quenched aluminum. It is apparent that samples with machining distortion can have complex surface shapes, where Bézier Surfaces and Gaussian Curvature provide more information than the commonly used 2D line plot data.

2012 ACM Subject Classification Applied computing → Engineering

Keywords and phrases Machining distortion, Metrology, Gaussian curvature

Digital Object Identifier 10.4230/OASIcs.iPMVM.2020.5

Funding *Destiny R. Garcia*: partially funded by NSF award No. 1663341.
Barbara S. Linke: partially funded by NSF award No. 1663341.

Acknowledgements Thank you to Michael Hill, UC Davis for guiding the machining distortion research. Many thanks to Christopher D'Elia and Renan Ribeiro, both UC Davis, for designing and machining the samples. We express our sincere thanks to Jan Aurich, Benjamin Kirsch, and Daniel Weber at TU Kaiserslautern for discussing the distortion application. All above mentioned researchers are collaborators on the *NSF/DFG Collaboration to Understand the Prime Factors Driving Distortion in Milled Aluminum Workpieces*, funded through NSF Award No. 1663341 and DFG Project No. 351381681. We also thank Jörg Seewig from TU Kaiserslautern for the helpful discussions on metrology. We furthermore interact in the IRTG 2057 *Physical Modeling for Virtual Manufacturing Systems and Processes*, funded by DFG.

Nomenclature

x, y, z	Cartesian coordinates
a, b, c	constants
z_{min}, z_{max}	minimum & maximum z heights
R	range of z heights
$b_k^n(t)$	degree n Bernstein basis functions

[1] Corresponding author

2nd International Conference of the DFG International Research Training Group 2057 – Physical Modeling for Virtual Manufacturing (iPMVM 2020).
Editors: Christoph Garth, Jan C. Aurich, Barbara Linke, Ralf Müller, Bahram Ravani, Gunther Weber, and Benjamin Kirsch; Article No. 5; pp. 5:1–5:17

OpenAccess Series in Informatics
Schloss Dagstuhl – Leibniz-Zentrum für Informatik, Dagstuhl Publishing, Germany

$x_{\min}, x_{\max}$ minimum & maximum x coordinate
$y_{\min}, y_{\max}$ minimum & maximum y coordinate
E least–squares–fit error function
c_{kl} coefficients of least–squares function
μ, ν matrix element indices
$M_{\mu,\nu}$ least–squares matrix elements
r_μ least–squares vector elements
$\mathbf{r}(u, v)$ vector parametric surface
$\mathbf{n}$ surface unit normal vector
E, F, G surface first fundamental form coefficients
L, M, N surface second fundamental form coefficients
K surface Gaussian curvature
$f(x, y)$ functional surface
z_{rms} root–mean–square surface height

1 Introduction

In the aerospace and manufacturing industries, billions of dollars are attributed to costs from reworking, remanufacturing, and/or rejecting components that are defective due to machining distortions [3] [28]. Machining distortion is the deviation of part shape from the original intent after machining and being released from a fixture [6]. Residual stresses locked into the workpiece are a primary factor contributing to machining distortions, coming from prior material processing steps such as rolling, forging, heat treating, etc. Residual stress develops from three main mechanisms: non-uniform plastic deformation, surface modification, and material phase and/or density changes [4] [29]. After processing, the residual stresses can cause deformation due to the re-equilibration of the tensile and compressive stresses to arrive at mechanical equilibrium within the whole volume of material [4] [16]. Every year, the aerospace industry experiences significant loss in profits from part distortion [26]. Example components and processes are wing panels and other aerospace components from quenched aluminum, where deep pockets are removed by milling.

To tackle machining distortion, empirical trials and computational approaches are employed. For example, analytical models have been developed to predict the distortion of monolithic aerospace components [21]. A bending moment model for predicting shape deviation has shown useful in simple geometries [5]. A physics-based materials processing simulation revealed similar results compared to experimental data [2]. Similarly, a physics-based machining model incorporating dynamic cutting forces and tool compliance properties has been developed to predict in-process deflections along computer numeric control (CNC) machining tool paths [18]. An enhanced analytic elasto-plastic model which uses superposition of thermal and mechanical stresses, followed by relaxation procedures has been developed to predict residual stresses in machining [20]. However, in the distortion literature, basic information is missing about how distortion is practically characterized and therefore the results of experiments or modeling approaches are not easy to transfer between works of different researchers. More information is needed on the measurements themselves as well as data processing to enable easy transfer of results between distortion papers. In manufacturing research, experimentation and measurements are closely related, but they also are clearly distinct – to which measurements deserve to be viewed independently from the study of experimentation [24]. Measurements are not exact, but rather depend on multiple factors including the measurement procedure, the operator skill, the environment,

and more [1]. Measurements have an associated measurement uncertainty that is used in a central role to assess quality and quality standards [10]. There are many types of measuring principles related to production metrology including but not limited to stylus instrument, white-light interferometer, confocal microscope, focus variation microscopy, angular resolved scattering light sensor, pneumatic distance measurement, etc. [19]. There are advantages and disadvantages for each measuring principle and ultimately the measurement principle is selected based on requirements of the production.

The goal of this study is to *find a transparent way to collect, quantify, and analyze distortion data* to enhance the transferability of experimental and analytical results. The focus is on areal measurement data. An approach to characterizing machining distortion by the Gaussian curvature of a parametric Bézier surface, created by a least–squares fit, is demonstrated as a novel means to metrologically characterize distortion.

2 Metrology of distortion

Metrology in general is focused on design, maintenance, and improvements to technology to create accurate measurements [24]. Metrology has the potential to improve the capability of manufacturing processes in a production environment [25]. A measurement is obtained from a measurement process, which requires measurement variables, hardware, software, and human input to carry out the measurement [17].The introduction of measuring systems in a company or industry is often driven by the need to ensure a specific level of quality in manufacturing, using metrology for inspection purposes [25]. A measurement systems analysis or MSA, is used to characterize the measurement process [17].

2.1 Coordinate measuring machines

For many researchers the measurement instrument of interest for machining distortion research is the coordinate measuring machine (CMM). A CMM is a measuring system with a probing system and the capability to determine spatial coordinates on the surface of the measured part [8] [11] [22]. It combines measured points to form a feature using coordinate metrology. Coordinate metrology provides a scientific basis to carry out measurements and 3D geometric object imaging with the use of coordinate measuring systems [27]. Coordinate measuring machines are designed to measure size, form, and position deviations of a workpiece [22]. A CMM is equipped with a specific type of probing system – contact areal, optical profile, or multi-sensor profile/areal [27]. The probing systems can collect data as single points or a series of points by scanning the workpiece inside the measurement field [22]. Measurement of 3D objects marks the section of the space with the geometry of the measured object given as a point coordinate in a reference coordinate system [27]. Tactile probing systems have roughness limitations due to the stylus tip size diameter. There are many different techniques available for surface measurement analysis and it is important to understand the sample properties, limitations of each, and analysis required [7].

For machining distortion, a coordinate measuring machine may be considered the most universal tool for collecting distortion data, such that it is capable of measuring: a point, line, plane, circle, cylinder, cone, sphere, ellipse, step cylinder, slot, circular slot, parabola, paraboloid, torus, parallel planes, curve, surface, etc. To fully understand the capability of the measurement system, it needs to be analyzed with regard to repeatability, reproducibility, linearity, bias, stability, consistency, and resolution [17]. In the presented study, three industry-relevant coordinate measuring machines at our disposal were chosen with tactile and optical principles.

Table 1 Distortion research examples from the literature often show a vague description of the data collection and analysis methods used.

	[23]	[30]	[18]	[15]	[13]	[2]
Measurement Tool	Taylor Hobson Form Talysurf Scanner	Hexagon Micro HITE 3D CMM	CMM	Mistral 775 3D CMM	CMM	N/A
Measurement Technology	Tactile probe	Tactile probe	N/A	N/A	N/A	N/A
Distortion Visualization	Central line, length direction	Central line, length & width	N/A	3 lines in length equidistant	Grid opposite machined surface	N/A
Distortion Space	Profile	Profile	Area	Profile	Area	Profile
Distortion Analysis	N/A	N/A	N/A	N/A	N/A	N/A

2.2 Distortion characterization

To characterize distortion, workpiece data needs to be measured, processed and visualized. Currently in the literature, distortion measurement includes a variety of methods with regard to measurement tools, tool technology, and distortion space (profile vs. areal measurement) (see Table 1). The analysis methods for the data are often not reported on. Many of the methods used for displaying machining distortion in the literature include a linear or two-dimensional visual representation using a central line for critical distortion maximum areas. In general, distortion measurements and measurands can be described in many ways including:

- a single value (i.e. maximum distortion, average distortion),
- a single curve along a reference surface (usually along the longitudinal direction with maximum deviation noted),
- a collection of curves along a surface (e.g. in both longitudinal and transverse directions with distinct distortion values noted),
- uniformly spaced measurement schemes in both x and y coordinate directions with maximum and minimum values described, etc.

Distortion is often measured as a maximum value or peak–to–valley height on one or several lines across the part. Some researchers take the peak–to–valley height for the whole areal surface. A method for displaying and characterizing machining distortion as areal data with several filtering and fitting steps is described in our previous work [12]. The distortion is calculated from the difference of a reference area measured before and after machining (or pre– and post–). The reference area needs to be largely unaltered by the machining process. Instead of a pre– and post–machining measurement, the post–measurement can be sufficient as long as the reference initial distortion is negligible, i.e., the workpiece surface is flat. Measuring only the post-machining surface for the distortion makes it easier for the operator to collect data and calculate distortion. Also, part quality is defined as difference from the intended shape, which in this case would be the part dimensions as defined by the designer in the CAD drawing, which usually takes an ideal initial condition.

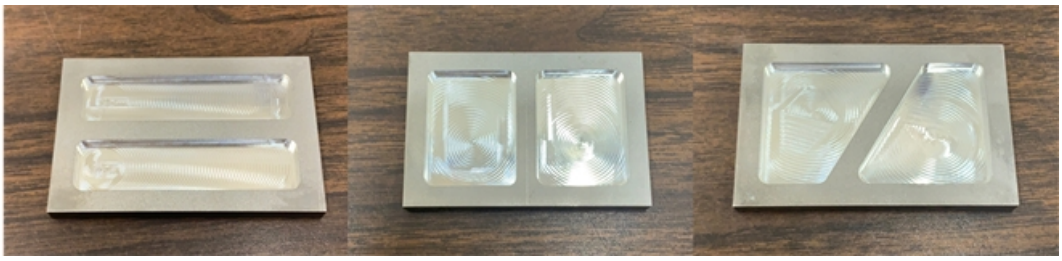

Figure 1 Distortion samples with machined pockets with 0, 90, 60-degrees stiffener walls [14].

Table 2 Specifications for the different CMM machines.

	Tactile CMM	Laser line and tactile probe CMM	Laser triangulation CMM
Model and Manufacturer	Mitutoyo Bright BRT504 CMM	FaroArm Edge & Scan Arm HD	Taylor Hobson Talyscan 250
Accuracy	0.0005 mm	0.029 mm	0.001 mm
Repeatability	0.003 mm	0.025 mm	**
Measurement Technology	Tactile Probe	Laser Line/Tactile Probe	Laser Triangulation
Measuring Capacity	$0.5 \times 0.4 \times 0.4$ m	$1.8 \times 1.8 \times 1.8$ m	$0.2 \times 0.2 \times 0.2$ m

3 Methods

3.1 Workpiece samples

Distortion data was collected on the reference surface (bottom surface) of three aluminum samples with machined pockets from a PAG quenched aluminum 7050 bar. The dimensions of each sample are 76.2 mm x 50.8 mm x 6.35 mm with two equally sized pockets around a stiffener wall at different angles from the sample edge as seen in Figure 1. The stiffener walls are at 0, 90 and 60 degrees. The samples were machined on a 3 axis Haas milling machine after near net shape blanks were cut out by wire-EDM. The pockets were machined with roughing parameters first (4 flute 30 degree helix 1/4" square end mill, trochoidal milling, at 3000 rpm, feed rate of 0.23 m/min, depth of cut of 1.27 mm) and finished with two wall finishing passes to achieve the corner radius (3 flute 30 degree helix 1/8" square end mill, contour milling, at 4500 rpm, feed rate of 0.51 m/min, first depth of cut of 0.38 mm, second depth of cut of 0.127 mm). Flood cooling with a water based coolant was used for all milling operations.

3.2 Coordinate Measuring Machines

Three CMMs were available at our disposal at the University of California Davis for this study: a Mitutoyo Bright BRT 504 CMM (tactile CMM), a Faro Arm Edge and Scan Arm HD CMM (laser line and tactile probe CMM), and a Taylor Hobson Talyscan 250 (laser triangulation CMM) as seen in Figure 2. Initial data collection was carried out on each CMM for investigation of measurement system capabilities and is described in the next section. The specifications and manufacturer technical capabilities of the metrology equipment are presented in Table 2. Note that the repeatability data for the Laser triagulation CMM is unavailable from the manufacturer's specification sheet.

Figure 2 Mitutoyo Bright BRT 504 - tactile CMM (left), Faro Arm Edge and Scan Arm HD - Laser line and tactile probe CMM (middle), and Taylor Hobson Talyscan 250 - Laser triangulation CMM (right).

3.3 Data collection and processing

Data was collected on the bottom surface of each sample, called the reference plane. We chose a single measurement scan instead of pre– and post–machining CMM measurements. The data was collected on each sample using each of the three CMMs for comparison. The comparability of the results was guaranteed because always the whole sample bottom surface was measured. Coordinate data from the CMMs was imported into Matlab software to be fit, leveled and plotted. A planar fit as seen in Equations (1) – (3) was used to level the raw data to the (x, y) plane (Equation (1)). The fit residual (distortion data minus the fitted data) provides leveled data for the following steps. Outliers in the leveled data were filtered further from the leveled data, where outliers are defined as z values near the extremes (maximum and minimum z values). The outliers were removed because they were not part of the measured surface. Instead, they were probing points falling off the edges of the physical part during the measurement. These points are very small percentage of total data points. Defining the z range R as maximum minus minimum (Equation (2)), outliers were identified and removed if outside the range of z from the data by Equation (3). Repeating the planar fit, leveling, and filtering steps three times provided a useful set of data, defined as having no significant outliers and with a difference between fit n and n+1 to be essentially zero. If pre– and post–data sets had been used, the data sets would have to be rotated, translated relative to each other and interpolated linearly to a common grid, before the difference of both data sets can be taken.

$$z(x, y) = a + bx + cy\,, \tag{1}$$

$$R = z_{max} - z_{min}\,, \tag{2}$$

$$z_{\min} + 0.015\,R < z < z_{\max} - 0.015\,R\,. \tag{3}$$

4 Optimizing the measurement parameters

In a first step, measurements were taken on the three above mentioned CMMs. The baseline spacing scheme for the x and y axes on the tactile CMM, and the laser triangulation CMM is 1×1 mm. The spacing scheme for the laser line and tactile probe CMM was found to be about 0.05 x 0.05 mm. Distortion data for each metrology equipment are shown for the

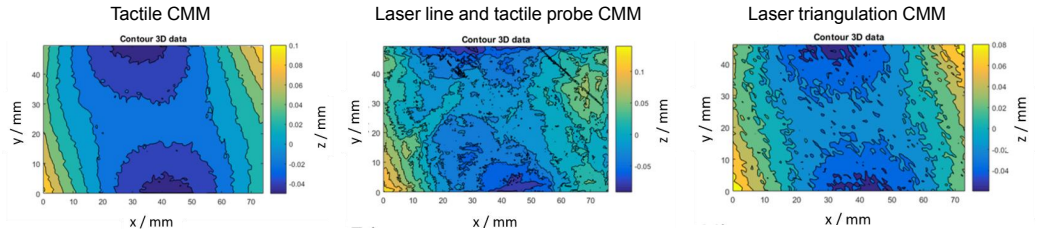

Figure 3 Distortion coordinate data of the sample with 60-degrees stiffener wall from three different CMMs.

60-degree sample in Figure 3. The distortion values (defined as the maximum z–deviations from the intended shape) varied for the different measurement machines and principles. If the scalar distortion values are defined as the maximum distortion value minus the minimum distortion value, the distortion results for the different tools are 0.2438 mm, 0.1504 mm, and 0.1535 mm for the laser line and tactile probe CMM, laser triangulation CMM, and tactile CMM respectively. The laser line and tactile probe CMM has a single point accuracy of 0.029 mm and a volumetric accuracy of ±0.041 mm which contributes to the data noise and to differences from the other coordinate measuring machines. The laser line and tactile probe CMM was therefore determined unfit for the following distortion measurement. The laser triangulation CMM exhibited optical difficulty with the reflective metal surface.

Further investigation of the distortion data from the machined pocket samples was conducted on the tactile CMM. The tactile CMM is often still considered the 'golden standard' in metrology as it represents a physical contact on the workpiece and has the longest history of standardization. The final distortion represents the overall shape features, not the minute texture (i.e. surface roughness).

In a second step, the coordinate spacing for the tactile CMM was investigated to assure quality data with consideration of measurement time. The spacing in the x and y axes were kept uniform. Pitch and increment spacing for the x and y axes respectively were investigated at 5×5 mm, 2×2 mm, 1×1 mm, and 0.5×0.5 mm as seen in Figure 4. Between the 5 x 5 mm and 0.5 x 0.5 mm spacing the general distortion shape does not change. We see that the distortion follows the 60 degrees stiffener wall. But the finer spacing leads to a higher resolution and more information about the surface. However, this must be weighed against the measurement time, which decreases roughly with the square of the spacing distance. Considerable measurement time reduction is possible with the coarser spacing. For the following measurements in this study, a 1 x 1 mm spacing was used. Table 3 shows the available scanning parameters on the chosen measurement device as well as the recommended parameters for the study at hand.

5 Distortion data analysis

The processed distortion data is shown in Figure 5 as 3D plot on the left and line plots for the horizontal midline (y = 25.4 mm) and vertical midline (x = 38.1 mm). The vertical midline shows a convex shape, the horizontal midline a concave shape.

As a new data analysis step, the leveled data is also imported into a least–squares surface fitting program that creates a Bézier surface, whose shape may be characterized by analysis of its Gaussian curvature. An illustration of the coordinate data analysis steps are shown in Figure 6.

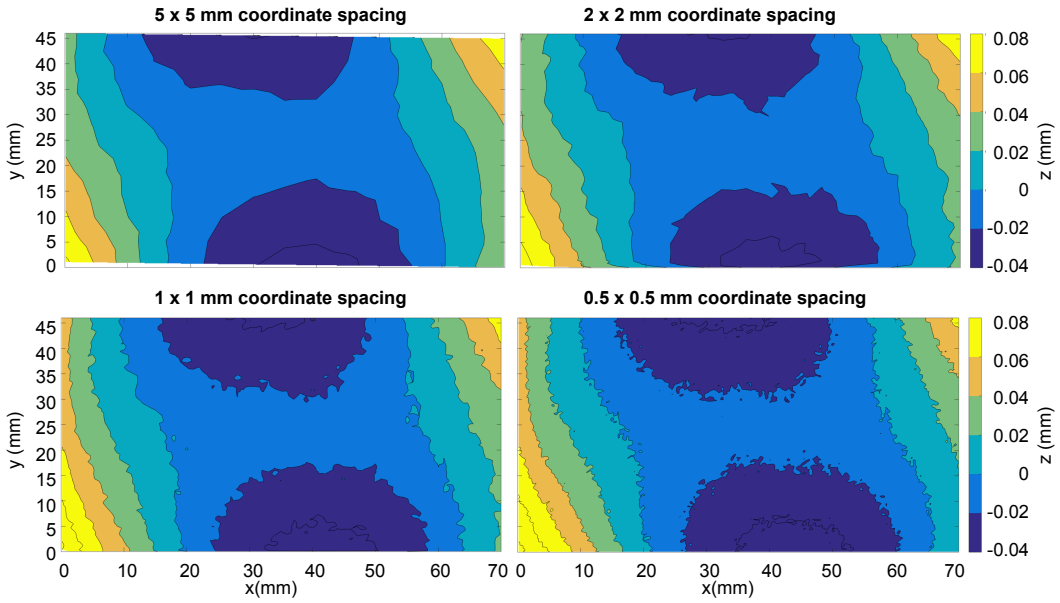

Figure 4 Distortion coordinate data of the sample with 60-degrees stiffener wall from the tactile CMM using different coordinate spacing schemes.

Table 3 Tactile CMM distortion measurement parameters.

CMM Scanning Parameter	**Definition or available options**	**Recommended Parameters**
x-spacing	Increment spacing between points in the x direction	1 mm
y-spacing	Pitch spacing between points in the y direction	1 mm
Lace feature	Repeat scan direction uniform or positive/negative direction	off
Scan method	Peck or Drag	Peck
Scan Transversal	x, y or z-axis	y-axis
Pecking axis	x, y, or z-axis	z-axis
Pecking direction	Positive or negative axis (x,y,z) direction	Negative z-axis
No. of T-patches	Length of the part / pitch	25
Retreat axis	x, y or z-axis	z-axis
Probe diameter	Size of the scanning probe ball diameter	4 mm
Probe Compensation	Coordinate datum is compensated using the radius of the scanning probe	On

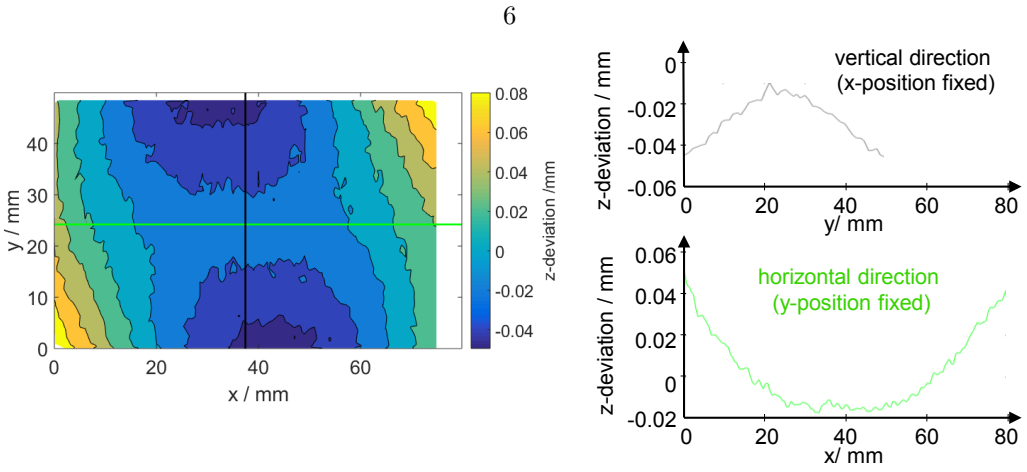

Figure 5 The leveled distortion data for the 60-degree sample with midline plots for both horizontal and vertical directions.

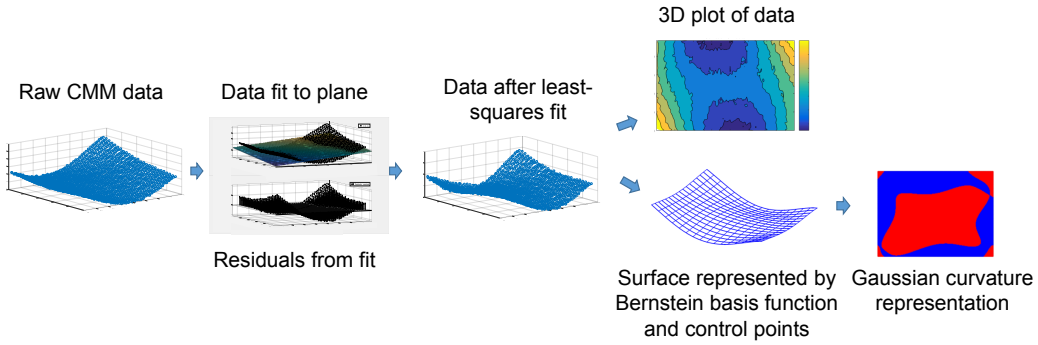

Figure 6 Steps for coordinate distortion data processing and visual representation.

After the data has been leveled, it is reduced to a uniform 500×500 2D grid using *meshgrid* and *griddata* in Matlab. The distortion is displayed as a contour plot. After leveling the data in Matlab, a least-squares method is used to remove any noise in the original coordinate data. The idea is to construct a Bézier surface with a grid of control points. The least-squares problem reduces to a linear system that is relatively easy to solve. The height distributions will give an idea about the local distortion shape (convex, saddle, etc.). The algorithmic steps for this optimized routine for characterizing machining distortion are presented below.

5.1 Least-Squares Fitting with Bézier Surfaces

Since the original leveled CMM coordinate data is noisy, it can be difficult to discern overall shape properties characterizing the distortion directly from it. To address this, we consider least–squares fitting of the data to polynomial Bézier surfaces to suppress the noise. The least–squares fit involves only the solution of a linear system of equations, and allows two–dimensional shape features of the data to be identified, rather than just properties along linear subsets (as with conventional methods).

The Bernstein polynomial basis of degree n over the interval $t \in [\,0,1\,]$ is defined by

$$b_k^n(t) \;=\; \binom{n}{k}(1-t)^{n-k}t^k\,, \quad k=0,\ldots,n\,,$$

and a polynomial $p(t)$ may be specified in terms of its Bernstein coefficients $c_0,\ldots,c_n$ through the expression

$$p(t) \;=\; \sum_{k=0}^{n} c_k b_k^n(t)\,.$$

The Bernstein basis has many advantageous properties [9] in the context of least–squares fitting of polynomials to noisy data over finite domains:

1. *unimodality*: $b_k^n(t)$ has a single maximum on $t \in [\,0,1\,]$;
2. *non–negativity*: $b_k^n(t) \geq 0$ on $t \in [\,0,1\,]$ for $k=0,\ldots,n$;
3. *partition of unity property*: $\sum_{k=0}^{n} b_k^n(t) = 1$ for all values of t;
4. *lower and upper bounds*: $\min_{0\leq k\leq n} c_k \leq p(t) \leq \max_{0\leq k\leq n} c_k$ for $t \in [\,0,1\,]$;
4. *variation–diminishing property*: the number R of real roots of $p(t)$ on $t \in (0,1)$ is less than the number $V(c_0,\ldots,c_n)$ of sign variations in its Bernstein coefficients by an even amount, i.e., $R = V(c_0,\ldots,c_n) - 2\,K$ for a non–negative integer K;
5. *differentiation and integration*: the derivative and the integral of $p(t)$ can be expressed as polynomials in Bernstein form of degree $n-1$ and $n+1$, respectively, with coefficients that are simple linear combinations of the coefficients $c_0,\ldots,c_n$;
6. *numerical stability*: the Bernstein basis is "optimally stable" among all non–negative polynomial bases on $[\,0,1\,]$ – i.e., it is impossible to construct a basis for which the values of $p(t)$ are systematically less sensitive to uniform relative perturbations of its coefficients.

A tensor–product Bézier surface $\mathbf{r}(u,v)$ of degree (d,d) on the domain $(u,v) \in [\,0,1\,]\times[\,0,1\,]$ is defined in terms of the Bernstein bases in the parameters u and v through its *control points* $\mathbf{p}_{kl}$ for $0 \leq k,l \leq d$ by the expression

$$\mathbf{r}(u,v) \;=\; \sum_{k=0}^{d}\sum_{l=0}^{d} \mathbf{p}_{kl}\, b_k^d(u) b_l^d(v)\,. \tag{4}$$

The least–squares surface fit of the leveled CMM coordinate data proceeds as follows. We are given the measured heights z_i at sample points (x_i,y_i) for $1 \leq i \leq N$ on the domain $(x,y) \in [\,x_{\min},x_{\max}\,] \times [\,y_{\min},y_{\max}\,]$. The Bernstein basis functions of degree d in x and y on $[\,x_{\min},x_{\max}\,]$ and $[\,y_{\min},y_{\max}\,]$ are defined by

$$b_k^d(x) \;=\; \binom{d}{k}\frac{(x_{\max}-x)^{d-k}(x-x_{\min})^k}{(\Delta x)^d}\,, \quad k=0,\ldots,d\,,$$

$$b_l^d(y) \;=\; \binom{d}{l}\frac{(y_{\max}-y)^{d-l}(y-y_{\min})^l}{(\Delta y)^d}\,, \quad l=0,\ldots,d\,,$$

where $\Delta x = x_{\max}-x_{\min}$, $\Delta y = y_{\max}-y_{\min}$. We wish to fit a (functional) tensor–product surface of degree (d,d) in (x,y) of the form

$$z \;=\; f(x,y) \;=\; \sum_{k=0}^{d}\sum_{l=0}^{d} c_{kl}\, b_k^d(x) b_l^d(y) \tag{5}$$

to the given data. The total squared error between the fitted surface and the given data is defined as

$$E \;=\; \sum_{i=1}^{N} \left[\, f(x_i, y_i) - z_i \,\right]^2 ,$$

and substituting from (equation 5) gives

$$E \;=\; \sum_{i=1}^{N} \left[\sum_{k=0}^{d} \sum_{l=0}^{d} c_{kl}\, b_k^d(x_i) b_l^d(y_i) - z_i \right]^2 .$$

The least–squares fit is obtained by minimizing the error E with respect to the coefficients c_{kl} of $f(x, y)$. Setting the derivative of E with respect to the coefficient c_{rs} equal to zero yields the equation

$$\frac{\partial E}{\partial c_{rs}} \;=\; \sum_{i=1}^{N} 2 \left[\sum_{k=0}^{d} \sum_{l=0}^{d} c_{kl}\, b_k^d(x_i) b_l^d(y_i) - z_i \right] b_r^d(x_i) b_s^d(y_i) \;=\; 0 \,,$$

or equivalently,

$$\sum_{k=0}^{d} \sum_{l=0}^{d} \left[\sum_{i=1}^{N} b_k^d(x_i) b_l^d(y_i) b_r^d(x_i) b_s^d(y_i) \right] c_{kl} \;=\; \sum_{i=1}^{N} b_r^d(x_i) b_s^d(y_i)\, z_i \,.$$

For each pair (r, s) with $0 \le r, s \le d$ this defines a system of $(d+1)^2$ linear equations for the unknown coefficients c_{kl} of the surface (Equation 5).

The linear equations can be solved by standard methods (e.g., Gaussian elimination). To do this, it is preferable to express the equations in standard matrix form. This is accomplished by setting

$$\mu = r(d+1) + s + 1 \quad \text{and} \quad \nu = k(d+1) + l + 1$$

for $0 \le r, s \le d$ and $0 \le k, l \le d$, so the linear equations can be written as

$$\sum_{\nu=1}^{(d+1)^2} M_{\mu\nu}\, \tilde{c}_\nu \;=\; r_\mu \,, \quad \mu = 1, \ldots, (d+1)^2$$

where the matrix elements, unknowns, and right–hand side values are

$$M_{\mu\nu} \;=\; \sum_{i=1}^{N} b_r^d(x_i) b_s^d(y_i) b_k^d(x_i) b_l^d(y_i) \,, \quad 1 \le \mu, \nu \le (d+1)^2 \,,$$

$$\tilde{c}_\nu \;=\; c_{kl} \,, \quad 1 \le \nu \le (d+1)^2 \,,$$

$$r_\mu \;=\; \sum_{i=1}^{N} b_r^d(x_i) b_s^d(y_i)\, z_i \,, \quad 1 \le \mu \le (d+1)^2 \,.$$

Once the solution vector $\tilde{c}_\nu$ for $\nu = 1, \ldots, (d+1)^2$ has been computed, it can be re–arranged as the two–dimensional array c_{kl} with $0 \le k, l \le d$ that defines the surface (Equation 5) by writing

$$c_{kl} \;=\; \tilde{c}_\nu \,, \quad \text{where} \;\; k = \lfloor (\nu - 1)/(d+1) \rfloor \,, \quad l = \nu - k(d+1) - 1 \,.$$

5.2 Surface curvature analysis

To analyze the shape of the surface with Equation (4) we must rely on *intrinsic* properties – i.e., shape measures that are independent of the surface parameterization. The *Gaussian curvature* is the most basic intrinsic measure of local surface shape. At every surface point, there exists a family of planes that contain the surface normal vector, each of which intersects the surface in a planar *normal section curve*. The curvature of each normal section curve specifies a *normal curvature* of the surface at a given point, and there are (in general) two mutually orthogonal orientations of the section planes for which the normal curvature is extremal. These section planes identify the *principal directions* and *principal curvatures* of the surface at each point, and the Gaussian curvature at each point is the product of the principal curvatures.

At a given point, a surface is "bowl–shaped" or "saddle–shaped" according to whether the Gaussian curvature at that point is positive or negative. For example, an ellipsoid has positive Gausssian curvature at every point, but a hyperboloid has negative Gaussian curvature at every point. A general "free–form" surface may exhibit regions of both positive and negative Gaussian curvature, separated by loci of zero Gaussian curvature called *parabolic lines*. Analysis of the Gaussian curvature of the distorted surfaces produced by machining can reveal whether they admit simple characterizations, or are inherently rather complex.

The coefficients of the *first fundamental form* of a parametric surface $\mathbf{r}(u, v)$ are defined in terms of its first partial derivatives as

$$E \,=\, \mathbf{r}_u \cdot \mathbf{r}_u \,, \quad F \,=\, \mathbf{r}_u \cdot \mathbf{r}_v \,, \quad G \,=\, \mathbf{r}_v \cdot \mathbf{r}_v \,.$$

The *second fundamental form* has coefficients given in terms of the surface normal vector

$$\mathbf{n} \,=\, \frac{\mathbf{r}_u \times \mathbf{r}_v}{|\, \mathbf{r}_u \times \mathbf{r}_v \,|}$$

and the surface second partial derivatives by

$$L \,=\, \mathbf{n} \cdot \mathbf{r}_{uu} \,, \quad M \,=\, \mathbf{n} \cdot \mathbf{r}_{uv} \,, \quad N \,=\, \mathbf{n} \cdot \mathbf{r}_{vv} \,.$$

The Gaussian curvature is determined in terms of the coefficients of the first and second fundamental forms as

$$K \,=\, \frac{LN - M^2}{EG - F^2} \,.$$

Hence, a neighborhhod of a point is "bowl–shaped" or "saddle–shaped" according to whether $K > 0$ or $K < 0$, while $K = 0$ identifies points on a parabolic lines (a surface with $K \equiv 0$ is a *developable* surface – imagined as a thin material sheet, it can be "flattened" onto a plane without stretching or compressing the material).

For the case of a "functional surface" specified as $z = f(x, y)$ we may take $u = x$, $v = y$ and the parameterization has the form $\mathbf{r}(x, y) = (x, y, f(x, y))$ with the properties

$$\mathbf{r}_x \,=\, (1, 0, f_x) \,, \quad \mathbf{r}_y \,=\, (0, 1, f_y) \,, \quad \mathbf{n} \,=\, \frac{(-f_x, -f_y, 1)}{\sqrt{f_x^2 + f_y^2 + 1}} \,,$$

$$\mathbf{r}_{xx} \,=\, (0, 0, f_{xx}) \,, \quad \mathbf{r}_{xy} \,=\, (0, 0, f_{xy}) \,, \quad \mathbf{r}_{yy} \,=\, (0, 0, f_{yy}) \,,$$

$$(E, F, G) \,=\, (f_x^2 + 1, f_x f_y, f_y^2 + 1) \,, \quad (L, M, N) \,=\, \frac{(f_{xx}, f_{xy}, f_{yy})}{\sqrt{f_x^2 + f_y^2 + 1}} \,,$$

$$K = \frac{f_{xx} f_{yy} - f_{xy}^2}{(f_x^2 + f_y^2 + 1)^2} \,. \tag{6}$$

After successfully implementing the optimized routine for characterizing machining distortion via Gaussian surface curvature, the results are displayed below.

6 Results and Discussion

The leveled data shown in Figure 5 depicts more information in the left contour plot, than in the two midline plots on the right. The distortion seen in the 60-degree sample is symmetric and complex; both of these properties are not evident from the line plots. Areal data yields more information for the user than profile data. But still the surface shape cannot easily be described from the depicted 3D plot.

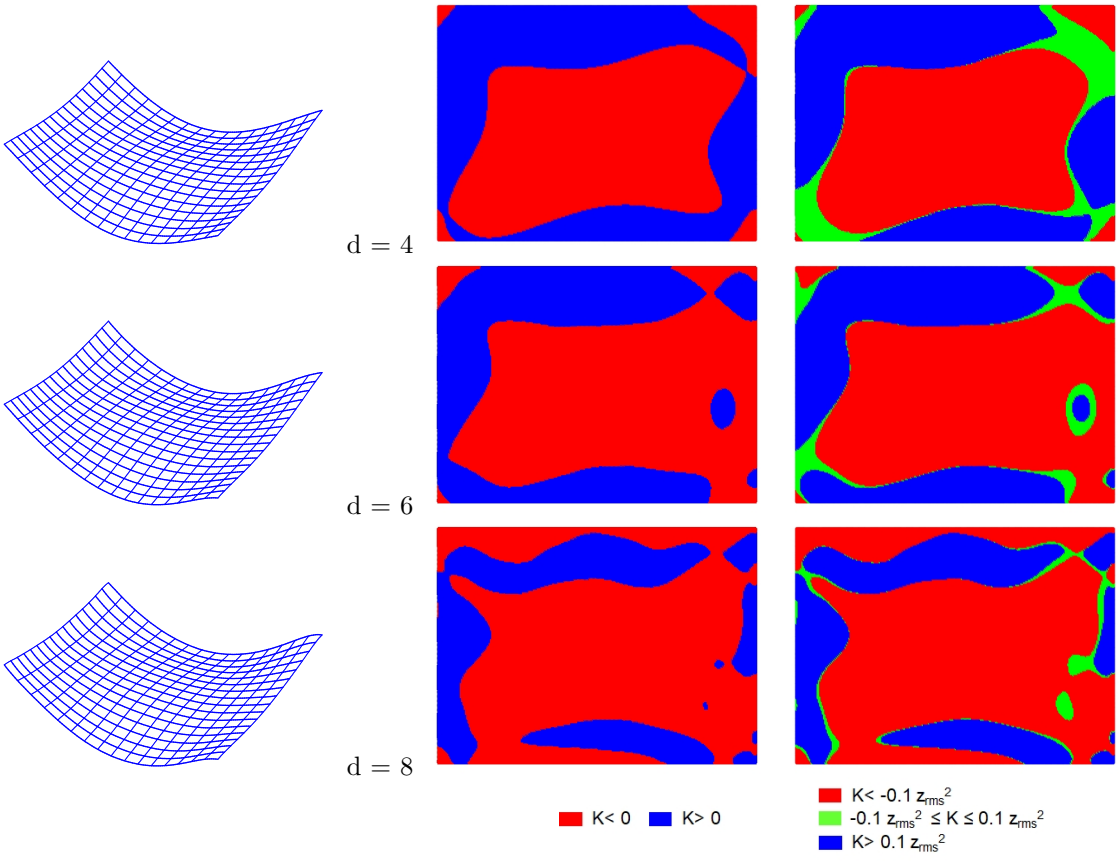

Figure 7 Least–squares surface fits with degrees $d = 4$ (top), $d = 6$ (center), and $d = 8$ (bottom). Left: height deviation of least–squares surface about the mean height (magnified 120×). Center: surface regions with negative (red) and positive (blue) Gaussian curvature K. Right: surface regions that satisfy $K > 0.1\, z_{\text{rms}}^2$ (blue), $-0.1\, z_{\text{rms}}^2 \le K \le 0.1\, z_{\text{rms}}^2$ (green), and $K < -0.1\, z_{\text{rms}}^2$ (red).

The leveled data was also used to compute a least–squares surface fit. From the leveled data of $N = 3825$ data points, the Gaussian curvature Equation (6) of the fitted surface was computed. Figure 7 shows the regions of positive and negative Gaussian curvature of the

fitted surface Equation (5) with degrees $d = 4, 6, 8$. Because the data points represent only a very mild deviation from planarity, the identification of these regions is sensitive to the number $(d+1)^2$ of fitting parameters – as d is increased, the fitted surface begins to more accurately replicate the noise inherent in the measured data.

Figure 7 also gives an alternative view, in which regions of low Gaussian curvature magnitude $|K| < 0.1\, z_{\text{ms}}^2$ (where z_{rms} is the root–mean–square deviation of the z heights) are color–coded green, while regions with $K > 0.1\, z_{\text{ms}}^2$ and $K < -0.1\, z_{\text{ms}}^2$ are colored red and blue. The green regions are nearly developable, indicating that the surface shape results from "bending" (rather than stretching or compressing) of an initially flat surface.

Figure 8 shows the magnified surface deviations and Gaussian curvature variations for the three test parts illustrated in Figure 1. A strong correlation of the curvature with the orientation of the stiffening wall is apparent. Overall, Figures 7 and 8 suggest that the surface distortions produced by machining are rather complex in nature, and do not admit characterization by simple, intuitive shape parameters.

Using the Gaussian curvature in addition to the areal distortion representation provides greater insight into the the overall surface deviation in the context of distortion analysis. Lower degrees d of the surface in the x and y directions impart a simpler impression of the overall distorted surface shape. As d increases, more features related to surface topography (i.e. surface roughness) are emphasized. Reducing the degree d incurs a smoothing effect that emphasizes the broad surface shape: as $(d+1)^2$ approaches N (the number of data points), the least–squares fit attempts to exactly interpolate every data point, yielding a Gaussian curvature distribution that is noisy, reflecting the surface roughness. Distortion data presented as either as a line or curve only exhibits a fraction of the overall experienced distortion on that sample. Two–dimensional data gives a sparse indication of the shape and does not adequately represent the complexity of the distorted shape.

7 Conclusion

This study explains an updated routine for characterizing machining distortion to improve comparison and transfer of distortion research between different studies. The optimized routine for characterizing machining distortion can be seen as a process to investigate the complexities of the unique distorted surface. The overall characterization process as seen in Figure 6 shows the steps to analyze distortion with Bézier surfaces and Gaussian curvature. Different representations of distortion will present more information about the distortion than just a single line plot or a single 3D image and help to understand machining distortion better.

Through this research, it is understood that distortion often includes complex shapes with regions of the surface between positive and negative Gaussian curvature. A new transparent way to characterize distortion via Gaussian curvature proves to be a simple method to transfer distortion results. Using the Bernstein basis function as a means for the least-squares surface fit for Gaussian curvature extraction of distorted machined samples, expresses a novel method to characterize machining distortion for the overall complex shape deviation. Extracting information from the curvature including symmetries, quantified positive and negative distributions, curvature location with respect to machined geometry, etc., can be useful for further distortion characterization and minimization.

More work is needed using Gaussian curvature characterization to expand the distortion results to show surface curvature symmetries, curvature percentages of both positive and negative curvatures, and distinct characterization Gaussian shapes for different distorted

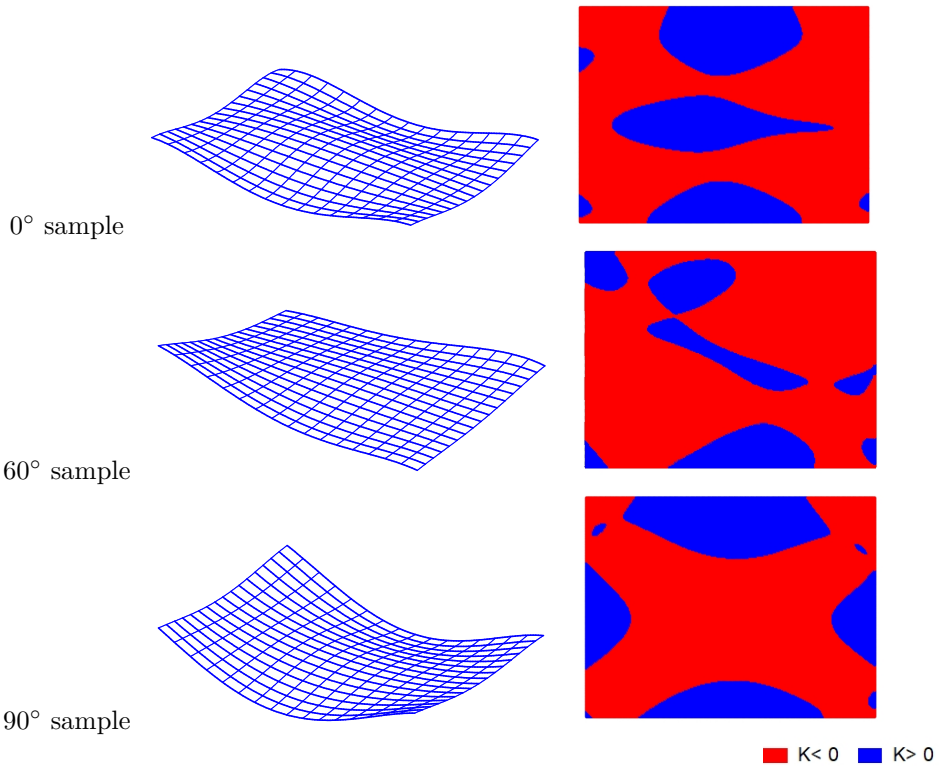

Figure 8 Left: height deviation of least–squares surface fit from the mean height (magnified 120×) for degree $d = 4$ surfaces. Right: plots showing regions of negative (red) and positive (blue) Gaussian curvature. The upper case shows the 0° *sample*; the middle case is the 60° *diagonal sample*; and the lower case is the 90° *sample*.

parts. Further work is also necessary in distortion compensation and distortion control. For example, Finite Element Analysis of distortion from residual stresses can use Gaussian Curvature to describe the distorted surfaces and can then be compared to Gaussian Curvature data from measured surfaces. Using the final distorted curvatures can allow for the prediction and manipulation of future machining distortion minimization. Future work is also needed to investigate more geometries and dimensions (i.e. complex geometries and pockets).

References

1 S. Bell. *Measurement Good Practice Guide No. 11. A Beginner's Guide to Uncertainty of Measurement.* Tech. rep., National Physical Laboratory, 1999.

2 Yun-bo Bi, Qun-lin Cheng, Hui-yue Dong, and Ying-lin Ke. Machining distortion prediction of aerospace monolithic components. *Journal of Zhejiang University-SCIENCE A*, 2009. doi:10.1631/jzus.a0820392.

3 DM Bowden and JE Halley. *Aluminum reliability improvement program final report 60606.* The Boeing Company, Chicago, IL, USA, 2001.

4 E. Brinksmeier, J.T. Cammett, W. König, P. Leskovar, J. Peters, and H.K. Tönshoff. Residual stresses — measurement and causes in machining processes. *CIRP Annals*, 31(2):491–510, 1982. doi:10.1016/S0007-8506(07)60172-3.

5 E. Brinksmeier and Jens Sölter. Prediction of shape deviations in machining. *CIRP Annals*, 58:507–510, December 2009. doi:10.1016/j.cirp.2009.03.123.

6 D. Chantzis, S. Van der Veen, J.Zettler, and W.M. Sim. An industrial workflow to minimise part distortion for machining of large monolithic components in aerospace industry. *Procedia CIRP*, 8:281–286, 2013. 14th CIRP Conference on Modeling of Machining Operations (CIRP CMMO). doi:10.1016/j.procir.2013.06.103.

7 M Conroy and J Armstrong. A comparison of surface metrology techniques. *Journal of Physics: Conference Series*, 13:458–465, 2005.

8 Richard Leach David Flack, James Claverley. Chapter 9 - coordinate metrology. In Richard Leach, editor, *Fundamental Principles of Engineering Nanometrology (Second Edition)*, Micro and Nano Technologies, pages 295–325, Oxford, 2014. William Andrew Publishing. doi:10.1016/B978-1-4557-7753-2.00009-8.

9 Rida T. Farouki. The bernstein polynomial basis: A centennial retrospective. *Computer Aided Geometric Design*, 29(6):379 – 419, 2012. doi:10.1016/j.cagd.2012.03.001.

10 Joint Committee for Guides in Metrology. *JCGM 104:2009. Evaluation of measurement data – An introduction to the "Guide to the expression of uncertainty in measurement" and related documents*, volume First edition. JCGM, 2009.

11 International Organization for Standardization. ISO 10360-1:2000 geometrical product specifications (gps) — acceptance and reverification tests for coordinate measuring machines (cmm) — part 1: Vocabulary). *Vernier, Geneva, Switzerland*, 2000.

12 Destiny R. Garcia, Michael R. Hill, Jan C. Aurich, and Barbara S. Linke. Characterization of machining distortion due to residual stresses in quenched aluminum. *Proceedings of the ASME 2017 12th International Manufacturing Science and Engineering Conference collocated with the JSME/ASME 2017 6th International Conference on Materials and Processing*, Volume 1: Processes, June 2017. V001T02A031. doi:10.1115/MSEC2017-2878.

13 M. Gulpak, J. Sölter, and E. Brinksmeier. Prediction of shape deviations in face milling of steel. In *Procedia CIRP*, 2013. doi:10.1016/j.procir.2013.06.058.

14 Michael Hill, Christopher D'Elia, Renan Ribeiro, and Julianne Emily Jonsson. Measurement and prediction of distortion from bulk residual stress in aluminum 7050 coupons (in preparation). *TBD*, 2021.

15 Xiaoming Huang, Jie Sun, and Jianfeng Li. Finite element simulation and experimental investigation on the residual stress-related monolithic component deformation. *International Journal of Advanced Manufacturing Technology*, 2015. doi:10.1007/s00170-014-6533-9.

16 Rémi Husson, Jean-Yves Dantan, Cyrille Baudouin, Serge Silvani, Thomas Scheer, and Régis Bigot. Evaluation of process causes and influences of residual stress on gear distortion. *CIRP Annals*, 61(1):551–554, 2012. doi:10.1016/j.cirp.2012.03.106.

17 ASTM International. ASTM E2782-17 standard guide for measurement systems analysis (msa). *West Conshohocken, PA*, 2017. doi:10.1520/E2782-17.

18 S. Jayanti, D. Ren, E. Erickson, Shuji Usui, T. Marusich, K. Marusich, and H. Elanvogan. Predictive modeling for tool deflection and part distortion of large machined components. *Procedia CIRP*, 12:37–42, December 2013. doi:10.1016/j.procir.2013.09.008.

19 Fritz Klocke. *Manufacturing Processes 1*. Springer Berlin Heidelberg, 2011. doi:10.1007/978-3-642-11979-8.

20 Ismail Lazoglu, Durul Ulutan, B. Alaca, Serafettin Engin, and Bilgin Kaftanoğlu. An enhanced analytical model for residual stress prediction in machining. *CIRP Annals - Manufacturing Technology*, 57:81–84, December 2008. doi:10.1016/j.cirp.2008.03.060.

21 Jian-guang Li and Shu-qi Wang. Distortion caused by residual stresses in machining aeronautical aluminum alloy parts: recent advances. *The International Journal of Advanced Manufacturing Technology*, 89:997–1012, March 2017. doi:10.1007/s00170-016-9066-6.

22 Karsten Luebke. Coordinate measuring machine. In Luc Laperrière and Gunther Reinhart, editors, *CIRP Encyclopedia of Production Engineering*, pages 285–289, Berlin, Heidelberg, 2014. Springer Berlin Heidelberg. doi:10.1007/978-3-642-20617-7_6579.

23 Ninshu Ma and Hui Huang. Efficient simulation of welding distortion in large structures and its reduction by jig constraints. *Journal of Materials Engineering and Performance*, 26:5206–5216, 2017.

24 Daniel Jon Mitchell, Eran Tal, and Hasok Chang. The making of measurement: Editors' introduction. *Studies in History and Philosophy of Science Part A*, 65-66:1–7, 2017. The Making of Measurement. doi:10.1016/j.shpsa.2017.10.001.

25 Enrico Savio, L. Chiffre, Simone Carmignato, and J. Meinertz. Economic benefits of metrology in manufacturing. *CIRP Annals - Manufacturing Technology*, 65:495–498, January 2016. doi:10.1016/j.cirp.2016.04.020.

26 Wei-Ming Sim. Challenges of residual stress and part distortion in the civil airframe industry. *International Journal of Microstructure and Materials Properties*, 5, December 2010. doi:10.1504/IJMMP.2010.037621.

27 Jerzy A. Sładek. *Coordinate Metrology*. Springer Berlin Heidelberg, 2016. doi:10.1007/978-3-662-48465-4.

28 Klaus-Dieter Thoben, Thomas Lübben, Brigitte Clausen Christian Prinz, Alwin Schulz, Rüdiger Rentsch, Ralf Kusmierz, Lutz Nowag, Holger Surm, Friedhelm Frerichs, Martin Hunkel, Dieter Klein, and Peter May. Distortion Engineering: Eine systemorientierte Betrachtung des Bauteilverzugs. *HTM - Haerterei-Technische Mitteilungen*, 57:276–282, April 2002.

29 PF FEng Y Ma, S Liu and DW Yu. Finite element analysis of residual stresses and thin plate distortion after face milling. In *12th International Bhurban Conference on Applied Sciences and Technology (IBCAST), Islamabad*, pages 67–71, 2015. doi:10.1109/IBCAST.2015.7058481.

30 Zheng Zhang, Liang Li, Yinfei Yang, Ning He, and Wei Zhao. Machining distortion minimization for the manufacturing of aeronautical structure. *International Journal of Advanced Manufacturing Technology*, 2014. doi:10.1007/s00170-014-5994-1.